Surrogate-Assisted Multi-Objective Optimization of Regional Turboprop Configurations with Rear-Mounted Propulsion and Three-Lifting-Surface Architectures

Stephen Howard Davis[1,*] and Frank M. White[1]

[1] Walter P. Murphy Professor Emeritus of Engineering Sciences and Applied Mathematics, Northwestern University

* Correspondence: sdavis@northwestern.edu

Abstract: Designing advanced regional turboprop airplanes involves addressing the aerodynamic efficiency, structural mass, fuel burn, longitudinal stability, and field performance within a constrained interplay. The paper investigates three different layouts for regional turboprops: standard wing-mounted engines; rear-mounted engines in which the propulsion system is mounted close to the horizontal tailplane; and three-lifting surfaces with a canard. Variables and design spaces for each layout are characterized via wing planform and horizontal-tail geometry; additionally, canard variables are considered when appropriate. Contrary to the approach of exhaustively searching a design space using a full-factorial design, this research applies the surrogate-based multi-objective optimization approach that employs Latin hypercube sampling, Gaussian-process regression modeling, and NSGA-II algorithm. Mission fuel mass, empty aircraft weight, and Direct Operating Cost proxy are the objectives that need to be minimized under a set of constraints related to static stability, takeoff and landing field lengths, climb time, cruise Mach number, landing-gear clearance in terms of aft center-of-gravity location, and fuel tank capacity. Results show that the rear-mounted propulsion helps achieve greater fuel-efficiency due to better wing aerodynamics, but suffers from additional horizontal-tail penalties. Three-lifting-surface configuration appears to provide optimal balance between fuel burn and performance parameters, provided that the canard placement and relative position of wings are chosen properly. The research concludes that the surrogate-based multi-objective optimization methodology presents a powerful method for preliminary aircraft design, in particular for nonstandard regional turboprop airplanes.

Keywords: regional turboprop aircraft; multidisciplinary design optimization; Gaussian-process surrogate; NSGA-II; rear-mounted propulsion; three-lifting-surface aircraft

Citation: Stephen Howard Davis and Frank M. White. 2021. Surrogate-Assisted Multi-Objective Optimization of Regional Turboprop Configurations with Rear-Mounted Propulsion and Three-Lifting-Surface Architectures. *TK Techforum Journal (ThyssenKrupp Techforum)* 2021(2): 18–32.

Received: March-22-2021
Accepted: August-09-2021
Published: Sptember-30-2021

1. Introduction

While regional turboprops have been eclipsed by regional jet aircraft in recent decades, they continue to represent a good choice for certain short-to-medium range missions due to their low fuel consumption compared to regional jets while retaining the ability to use secondary airports. The challenge of the design problem arises from the fact that a regional turboprop aircraft is not just a collection of independent aerodynamic, structural, and performance decisions. Engine installation affects drag and mass-relief characteristics of the wing, wing longitudinal placement alters the center-of-gravity corridor, landing-gear location, and trim requirement, while the introduction of the forward lifting surface brings additional load-sharing advantages, along with new downwash and stability interactions. Therefore, the conceptual design problem is ideally suited to a multidisciplinary design optimization approach, rather than sequential sizing [1–3].

Conventional wing-mounted configurations have several practical benefits: engine mounting is structurally conventional, there is sufficient ground clearance of the propeller,

the engine mass relieves the wing, and certificational practices are well-developed. Disadvantages of the conventional layout primarily come from nacelle-wing interference, the drag of landing-gear fairings, and a lack of potential for clean wing aerodynamics. In turn, the rear-mounted layout eliminates interference between turboprops and the wing, but it also imposes additional inertial and vibratory loads to the aft-fuselage and empennage structure. Hence, the rear-mounted propulsion must be evaluated with simultaneous improvements in fuel mass, empty weight, stability margin, takeoff distance, and operation cost [4–6].

Three-lifting-surface aircraft have another option worth consideration. As the canard lifting surface carries some lift and relieves the horizontal stabilizer from longitudinal trim forces, it allows reducing trim drag, provided the arm and level of lift are consistent with main wing and tail geometry. On the other hand, wind tunnel and computational experiments reveal that the additional forward surface may modify the downwash field at the horizontal tail and, potentially, affect the aircraft directional stability via vortex interaction between canard, wing, and tail [7,8]. In other words, while the canard is not inherently advantageous, it proves to be so when located within a special design corridor, where trim relief, stability, fuel volume, and structure all work together in favor of the design.

In the literature, there are numerous methodologies for estimating the performance, weight, balance, and stability of aircraft concepts [9–11]. Meanwhile, the literature on multidisciplinary design optimization demonstrates that optimization of a multi-disciplinary problem typically leads to poor efficiency for exhaustive full-factorial enumeration due to rapid increase in number of design points [12,13]. An effective way to overcome such challenges is surrogate modeling and analysis, which consists of generating an inexpensive statistical response function and improving its accuracy near the areas of interest (e.g., Pareto frontier) via expensive multidisciplinary analysis [14–16]. Gaussian process regression has proven its effectiveness in conceptual aircraft design due to its prediction accuracy, along with a possibility to estimate local response variance, while NSGA-II algorithm ensures reliable Pareto frontier search [17–19].

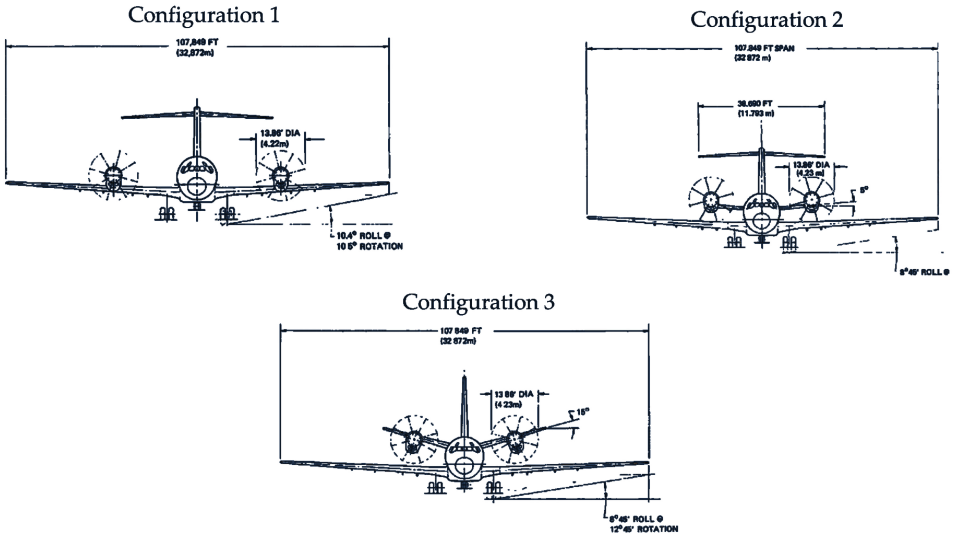

Figure 1. Configuration families considered in the design study: wing-mounted propulsion, rear-mounted propulsion, and a canard-wing-tail arrangement. The recolored linework emphasizes the alternative architecture families while keeping geometric details intact.

However, it is not clear if a combination of a surrogate-assisted optimization procedure will be able to recognize true configuration benefits from purely geometrical ones in a constrained multidisciplinary problem. The current paper explores the applicability of surrogating to three architectural concepts of turboprop aircraft. Specifically, it attempts

to find out if a rear-mounted propulsion configuration indeed has lower verified mission fuel mass than conventional design. It seeks to identify a preferable Pareto compromise of either a three-lifting-surface or a rear-mounted propulsion configuration. Finally, it tests if Gaussian process-assisted NSGA-II can find the non-dominated region with significantly less multidisciplinary runs than exhaustive enumeration.

The objectives of the paper are, thus, very specific. They determine the formulation of the multidisciplinary design problem, the optimization strategy, and interpretation of the results presented in the figures and tables below. Three architectural families considered in this work are depicted in Figure 1. This figure serves not only to demonstrate the geometrical difference between the configurations; it shows the physical origin of multidisciplinary optimization problem.

2. Configuration Space and Problem Definition

2.1. Aircraft configurations

The aircraft under consideration is analyzed using three different sets of aircraft configuration, represented by families A, B, and C. Configurations A represent traditional fixed-wing aircraft with turboprop engine at wing mounted position. Configuration B shifts the turboprop engine installation to the aft position and eliminates the presence of nacelle interference from the wing. Configurations C keep the propellers in the aft position, but incorporate a canard along with wing and vertical stabilizer as the other two lifting surfaces. The purposeful limitation of design parameters to only include those which will dominate in geometry, balance, drag and performance aspects is due to the nature of the analysis to be performed, i.e., to identify potential configuration level trade-offs without engaging in detailed structural certification design.

2.2. Variables of the design and bounds

Table 1 illustrates the values of design variables and corresponding allowable bounds. These design variables have been chosen because they can change the most important aerodynamics and longitudinal balancing properties of the vehicle during the optimization process.

Table 1. Configuration-dependent design variables and bounds used in the multidisciplinary design study.

Design variable	A: wing-mounted	B: rear-mounted	C: three-surface
Wing span b_W (m)	33.5–36.0	33.5–36.0	33.5–36.0
Wing aspect ratio AR_W	11.8–13.4	12.2–13.8	12.2–13.8
Wing leading-edge position $X_{LE,W}$ (m)	13.5–16.0	19.5–22.0	19.5–22.0
Wing leading-edge sweep $\Lambda_{LE,W}$ (deg)	0–4	0–4	0–4
Horizontal-tail span b_H (m)	10.2–11.2	12.4–13.8	12.4–13.8
Horizontal-tail position $X_{LE,H}$ (m)	37.15 fixed	30.0–32.0	30.0–32.0
Horizontal-tail aspect ratio AR_H	4.96 fixed	4.40 fixed	4.40 fixed
Horizontal-tail sweep $\Lambda_{LE,H}$ (deg)	$\Lambda_{LE,W} + 5$	$\Lambda_{LE,W} + 5$	$\Lambda_{LE,W} + 5$
Canard span b_C (m)	—	—	7.2–8.8
Canard longitudinal position $X_{LE,C}$ (m)	—	—	5.0–8.0
Canard aspect ratio AR_C	—	—	5.57 fixed
Canard sweep $\Lambda_{LE,C}$ (deg)	—	—	10 fixed

As seen in Table 1, configurations B and C are not merely perturbations of the conventional configuration. Both the rearward shift of the wing and reduction of the horizontal-tail arm length mean that different compromises must be found to satisfy the stability and clearance requirements, involving a different distribution of wing position, horizontal tail area, and structural mass. The use of canard variables for trimming purposes in the three-surface configuration adds another trim control variable, at the cost of increasing the number of degrees of freedom and potentially introducing nonlinear boundaries in terms of feasibility.

Assumptions relating to drag, weight, laminar flow, landing-gear arrangement, and tail loads are depicted in Figure 2. The recolored version of the figure makes these factors explicit, which are responsible for defining whether any aerodynamic advantages offered by configurations B and C survive multidisciplinary closure.

	Wing-Mounted Engines			Rear-Mounted Engines			Three-Lifting Surfaces		
Technology	**Weight**	**Drag**	**Lift and Long. Stability**	**Weight**	**Drag**	**Lift and Long. Stability**	**Weight**	**Drag**	**Lift and Long. Stability**
Wing NLF	-	-10dcs	-	-	-20dcs	-	-	-20dcs	-
 **Fuselage LG and pods**	+7%Fuselage	+15dcs (pods)	-	-	-	-	-	-	-
 **Under-wing engine**	-5%Wing	+ 10dcs	-0.2 C_{Lmax} Downwash at Htail 0.25 (at M=0.2)	-	-	-	-	-	-
 **Rear-mounted engine at Htail tip**	-	-	-	+5%Wing +4%Fuselage +65%Htail	-	+0.2 C_{Lmax} +10% C_{LaH} Downwash at Htail 0.32 (at M=0.2)	+5% Wing +4% Fuselage +65% Htail	-	+0.2 C_{Lmax} +10% C_{LaH} Wing-Tail downwash
 **Canard Installation**	-	-	-	-	-	-	+5% Fuselage	-	+0.15C_{Lmax} Downwash at Htail 0.53 (at M=0.2)

Figure 2. Configuration-dependent technology and installation assumptions. The restrained monochrome palette emphasizes differences in aerodynamics, weight, and installation without drawing undue attention to the color differences among wing-mounted, rear-mounted, and three-surface concepts.

2.3. Geometric and aerodynamic relations

For each lifting surface $i \in \{W, H, C\}$, the planform area and mean chord are given by

$$S_i = \frac{b_i^2}{AR_i}, \qquad \bar{c}_i = \frac{S_i}{b_i}. \tag{1}$$

As shown in Eq. (1), the geometric parameters directly determine the aerodynamic loading and internal volume. An increased value of b_W, assuming moderate changes of AR_W, leads to lower induced drag but higher empty weight due to structural reasons and decreased internal volume because of the wing structure and fuel-tank layout.

Cruise drag polar of the direct MDO model in simplified form reads

$$C_D = C_{D0} + \Delta C_{D,\text{inst}} + k(C_L - C_{L,0})^2 + \Delta C_{D,\text{trim}}, \tag{2}$$

where C_{D0} is the clean airframe parasite drag, $\Delta C_{D,\text{inst}}$ the installation drag, k is the induced drag constant, and $\Delta C_{D,\text{trim}}$ is the trim drag correction term. As shown in Eq. (2), reduction in $\Delta C_{D,\text{inst}}$ due to nacelles installation at the rear end explains why the rear-mounted configuration leads to lower fuel mass. Eq. (2) is also useful to understand how canards may improve aircraft performance by lowering trim drag $\Delta C_{D,\text{trim}}$.

Range relation for turboprop aircraft is used to express mission fuel in terms of aircraft efficiency:

$$R = \frac{\eta_p}{c_p}\left(\frac{L}{D}\right)_{cr} \ln\left(\frac{W_i}{W_f}\right). \tag{3}$$

The above equation may be written as the explicit dependence on mission fuel

$$m_{fuel,mission} = m_i \left[1 - \exp\left(-\frac{Rc_p}{\eta_p (L/D)_{cr}} \right) \right] + m_{reserve}. \tag{4}$$

In Eqs. (3) and (4), it is clear that fuel mass depends exponentially on aircraft range, propeller efficiency, specific fuel consumption, and the cruise lift-over-drag ratio. Improvements in $(L/D)_{cr}$ are therefore valuable, but only those which will not lead to higher weights W_i and higher mass fraction of mission fuel.

The longitudinal static stability is accounted for via the static margin

$$SM = \frac{x_{NP} - x_{CG}}{\bar{c}_W}, \tag{5}$$

with an approximation for the neutral point as follows

$$x_{NP} = \frac{a_W S_W x_W + \eta_H a_H S_H x_H + \eta_C a_C S_C x_C}{a_W S_W + \eta_H a_H S_H + \eta_C a_C S_C}. \tag{6}$$

If the canard is not used ($S_C = 0$), then Eq. (6) describes the neutral point position for two surfaces (W and H). The importance of the canard geometric parameter $X_{LE,C}$ as a shift of the neutral point in terms of pitch moment becomes obvious from Eqs. (5) and (6). However, use of canard must not lead to the situation where neutral point approaches the aft limit of the center of gravity movement.

Trim conditions are imposed with the following equation

$$\sum_{i \in \{W,H,C\}} q S_i C_{L,i} (x_i - x_{CG}) + q S_W \bar{c}_W C_{m,W} + T(z_T - z_{CG}) = 0. \tag{7}$$

This equation is key in understanding the difference between configurations considered in the paper. In conventional aircraft with a horizontal tail, this tail typically produces a pitching moment that helps keep the equilibrium, requiring possibly negative tail lift. In three-surface aircraft, some pitching moment may come from canard, reducing tail load and trim drag.

Feasibility of the mission fuel capacity is imposed with the following constraint

$$m_{fuel,mission} \leq \rho_f \eta_{tank} \int_{y_{in}}^{y_{out}} \tau(y) c^2(y)\, dy, \tag{8}$$

where ρ_f is the density of fuel, η_{tank} is the usable volume factor of the tanks, $\tau(y)$ is the thickness-chord ratio at a span station y, and $c(y)$ is the local chord. The rationale for the appearance of wing geometry multiple times in the sensitivity analysis to come can be explained by Eq. (8): not only does it affect induced drag, but also affects the volume of fuel that can be accommodated by the design mission.

Runway field lengths, formulated in the concept design normalized form, look as

$$S_{TO} \approx K_{TO} \frac{W/S_W}{\rho C_{L\,\max,TO} (T/W)}, \qquad S_L \approx K_L \frac{W/S_W}{\rho C_{L\,\max,L}}, \tag{9}$$

where K_{TO} and K_L collect operational and regulatory factors. Eq. (9) shows that wing loading is the main driver of runway demand, but in this study the result is also affected by rotation clearance, gear location, and longitudinal balance.

2.4. Assumptions based on each configuration

Assumptions for configuration A include the engine mounting on the wings, which relieves the wings of a structural requirement but adds nacelle-wing interference drag and denies the advantage of having a clean wing from an aerodynamic standpoint. On the other hand, in configuration B, we have a cleaner wing aerodynamically, yet the aft engine

mounting results in a more structural challenge for the empennage portion while at the same time making the center-of-gravity requirement harder to meet. In the case of configuration C, we maintain the same assumptions for rear propulsion and add a canard to aid with the sharing of the loads longitudinally. These parameters still need to be designed because optimal values will be reached when several constraints are simultaneously fulfilled such as the trim condition, static margin, downwash, and field performance constraints.

2.5. Design constraints and objective functions

All candidate designs must satisfy

$$SM_{\min} > 0, \tag{10}$$
$$S_{TO} \leq 1400 \text{ m}, \tag{11}$$
$$S_L \leq 1400 \text{ m}, \tag{12}$$
$$t_{climb}(1500 \text{ ft} \rightarrow 25{,}000 \text{ ft}) \leq 16 \text{ min}, \tag{13}$$
$$0.64 \leq M_{cruise} \leq 0.68, \tag{14}$$
$$X_{LG} - X_{CG,\max aft} \geq 0.05\bar{c}_W, \tag{15}$$
$$m_{fuel,mission} \leq m_{fuel,tank}. \tag{16}$$

The constraint set in Eq. (16) prevents the optimizer from selecting aerodynamically attractive but mechanically impractical aircraft. In particular, the gear-clearance and fuel-capacity inequalities are important because they couple geometric layout decisions to operational feasibility.

The optimization is formulated as

$$\min_{\mathbf{x}\in\Omega} \mathbf{f}(\mathbf{x}) = \Big[m_{fuel,mission}(\mathbf{x}),\ W_{empty}(\mathbf{x}),\ DOC^*(\mathbf{x})\Big], \tag{17}$$

subject to the constraints in Eq. (16). The cost proxy is written as

$$DOC^* = c_f m_{fuel,mission} + c_w W_{empty} + c_p P_{inst} + c_h W_H + c_r(S_{TO} + S_L), \tag{18}$$

where the coefficients weight fuel expenditure, structural maintenance, propulsion-installation complexity, horizontal-tail penalty, and field-length demand. Eqs. (17) and (18) avoid reducing the aircraft to a single fuel-burn calculation. They force the optimization to expose trade-offs among fuel efficiency, structural mass, integration complexity, and airport accessibility.

3. Multi-Objective Optimization Algorithm Using Surrogates

3.1. Reasons for surrogate-based optimization

It would take too many runs of the multidisciplinary analysis when varying position, wing span, aspect ratio, tail geometry, and canards to conduct a full-factorial search. The three surface configuration poses even greater challenges, since the introduction of canard variables leads to a larger design space and more non-linear feasible regions. In that respect, the current optimization process includes a space-filling initial sample, Gaussian process regression, NSGA-II optimization, and adaptive infill evaluation. Figure 3 depicts the multidisciplinary analysis path that will be followed when the design candidates undergo full multidisciplinary analysis.

Figure 3 highlights the reason behind the fact that one evaluation does not mean one drag calculation. Candidates need to go through the processes of weight estimation, balance computation, aerodynamic and stability analysis, performance assessment, fuel mission closure, and costs estimation. The surrogate modeling approach captures this overall multidisciplinary behavior.

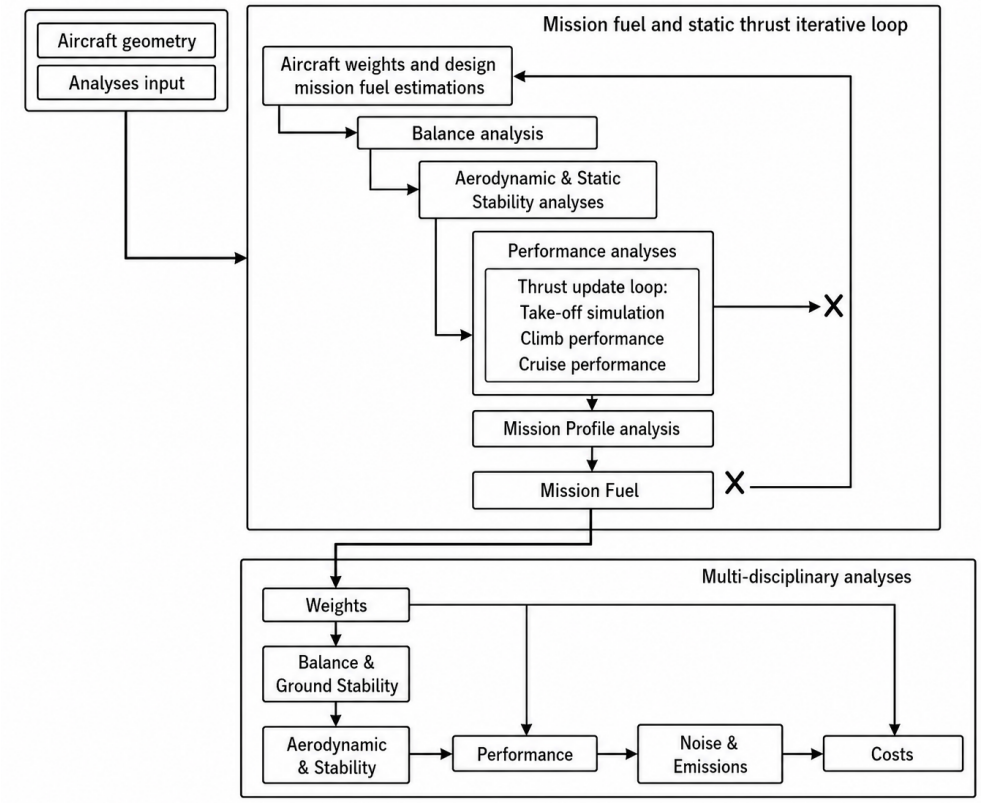

Figure 3. Multidisciplinary analysis path followed during each multidisciplinary design optimization step. Grayscale rendering is applied, since different colors distinguish the optimizer, mission loop, analysis modules, and constraints.

3.2. Sampling and direct evaluation

Latin hypercube sampling is used to generate an initial space-filling database. Sample sizes are 180, 260, and 340 samples for design families A, B, and C, respectively. The increasing sample size is in line with the increasing dimensionalities and nonlinear couplings in the respective design families. Violated constraints do not lead to discarding a candidate design; they are saved with the corresponding constraint violation degree to allow learning from infeasible designs as well.

3.3. Gaussian process response modeling

Denote the normalized design variable vector $\mathbf{x} \in \mathbb{R}^d$. The response $y(\mathbf{x})$ has the model

$$y(\mathbf{x}) = \mu(\mathbf{x}) + Z(\mathbf{x}), \qquad Z(\mathbf{x}) \sim \mathcal{GP}\big(0, k(\mathbf{x}, \mathbf{x}')\big), \tag{19}$$

where the kernel function $k(\mathbf{x}, \mathbf{x}')$ is chosen as the anisotropic squared exponential covariance kernel

$$k(\mathbf{x}, \mathbf{x}') = \sigma_f^2 \exp\left[-\sum_{i=1}^{d} \frac{(x_i - x_i')^2}{2\ell_i^2}\right] + \sigma_n^2 \delta_{\mathbf{x}\mathbf{x}'}. \tag{20}$$

As seen in Eq. (20), each design direction has its own length scale parameter ℓ_i. A small ℓ_i means that the design direction results in rapidly changing responses, as expected for variables such as the longitudinal wing position and canard placement.

The posterior prediction for a test input $\mathbf{x}_*$ given a training data set $\mathbf{y}$ from design matrix X is

$$\begin{aligned} \hat{\mu}(\mathbf{x}_*) &= \mu(\mathbf{x}_*) + \mathbf{k}_*^T K^{-1}(\mathbf{y} - \boldsymbol{\mu}), \\ \hat{s}^2(\mathbf{x}_*) &= k(\mathbf{x}_*, \mathbf{x}_*) - \mathbf{k}_*^T K^{-1} \mathbf{k}_*. \end{aligned} \tag{21}$$

The first term of Eq. (21) will be used for optimizing the response values, whereas the second one will be used when performing the surrogate model-based infill sampling step. This two-fold output is precisely the main benefit of employing Gaussian process regression over a pure deterministic approach in the present study.

3.4. Handling of constraints and Pareto search

Non-dominated Sorting Genetic Algorithm II is applied to surrogate responses via a population of size 160, simulated binary crossover probability equal to 0.90, polynomial mutation rate $1/d$, and tournament selection with constraint domination. Constraint violation can be expressed as follows:

$$CV(\mathbf{x}) = \sum_{j=1}^{n_g} \left[\frac{\max(0, g_j(\mathbf{x}))}{s_j} \right]^2, \tag{22}$$

where $g_j(\mathbf{x}) \leq 0$ represents the feasible variant of the jth constraint and s_j denotes the corresponding scaling constant. The use of such a criterion ensures preference for those solutions close to a constraint border over highly violating solutions, which is necessary when learning the small feasible domains for rear-mounted and three surface configurations.

3.5. Infill refinement with adaptability

In every 40-th generation, new candidates for re-evaluation are selected in accordance with

$$\Phi(\mathbf{x}) = \alpha\, EI_D(\mathbf{x}) + (1-\alpha) U_g(\mathbf{x}), \qquad \alpha = 0.65, \tag{23}$$

where EI_D is a dominance-based indicator of improvement and U_g is the uncertainty measure based on active criteria and constraints. A simplified expression for the latter is provided below:

$$U_g(\mathbf{x}) = \left[\sum_{r=1}^{n_f+n_g} \left(\frac{\hat{s}_r(\mathbf{x})}{s_r} \right)^2 \right]^{1/2}. \tag{24}$$

Formulas (23) and (24) quantify the trade-off between exploitation and exploration. It is encouraged to enhance the Pareto frontier, but it is also required to explore areas that are uncertain where the surrogate function approximation could be inaccurate at boundaries of feasibility.

3.6. Convergence criteria and algorithm description

Termination occurs whenever the relative hypervolume changes fulfill the criterion

$$\frac{HV^{(k)} - HV^{(k-1)}}{HV^{(k-1)}} < 0.01 \tag{25}$$

during three consecutive cycles of refinement. Formula (25) provides a realistic criterion for stopping since it does not need all the variables to converge; however, the space that is dominated by the Pareto optimal set should converge.

Algorithm 1: MDO of the regional turboprop configurations using surrogates

1. Choose architecture-specific design variables and corresponding ranges.
2. Create Latin hypercube samples for each configuration family.
3. Compute the objective values of initial samples using the direct analysis approach.
4. Develop Gaussian process models for the objectives and constraints.
5. Perform optimization using NSGA-II based on constraint domination.
6. Select infill samples based on dominance and uncertainty indices.
7. Re-optimize using the surrogate models with newly obtained samples.
8. Repeat steps five to seven until the relative hypervolume converges.
9. Validate solutions by using the direct multidisciplinary model.

4. Results and Discussion

4.1. Surrogate accuracy and computational efficiency

The surrogate models were stabilized by three successive stages of adaptive refinement. Table 2 shows the mean absolute percentage error of the final models. The errors stay within 4.2% for all presented response functions, which is acceptable for preliminary configuration ranking since their verified variations across configuration families exceed the remaining surrogate errors.

Table 2. Final surrogate model validation errors resulting from the surrogate-assisted design study.

Response	Wing-mounted	Rear-mounted	Three-surface
Mission fuel mass	2.4%	2.7%	2.8%
Empty weight	3.1%	3.4%	3.6%
Take-off field length	3.6%	3.9%	4.1%
Landing field length	3.0%	3.2%	3.5%
Climb time	2.9%	3.1%	3.3%
Static margin	3.7%	4.0%	4.2%

Table 2 is interpreted here not just as evidence of average accuracy of the surrogate model but also of its suitability for optimization. The highest surrogate errors belong to static margin and take-off, since they have geometric dependencies, gravity center displacement considerations, and constraints on aircraft rotation. These errors do not prevent Pareto optimization but give justification for the final verification run.

The saving in computational resources achieved compared to exhaustive exploration is shown in Table 3. It is increasing with respect to the number of design variables due to the exponential growth of the exhaustive enumeration space with design-space dimension and linear scaling of the surrogate-adaptive approach with design dimension.

Table 3. Number of direct analyses required by the exhaustive enumeration approach and by the surrogate-assisted one.

Configuration	Exhaustive evaluations	MDA calls	Saving
Wing-mounted	972	264	72.8%
Rear-mounted	6075	388	93.6%
Three-surface	34,020	516	98.5%

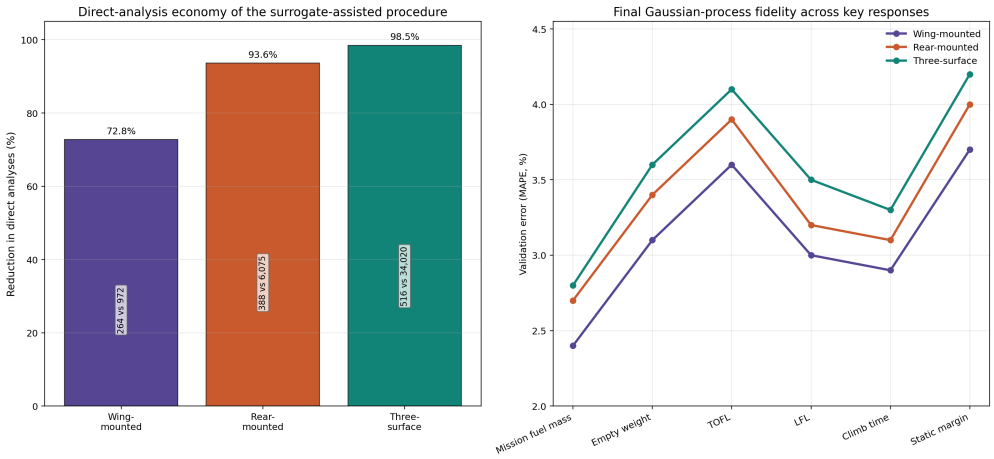

Figure 4. Computational economy and final validation accuracy of the surrogate-assisted procedure. The revised palette separates the three configuration families and improves readability of the bar and line trends.

The efficiency of the surrogate-assisted procedure and final validation errors are combined in Figure 4. The most important part of the figure is the three-surface case, where 516 MDA calls are sufficient to reduce exhaustive exploration by 34,020 calls and obtain approximate validation errors of about 2.8%-4.2%. This confirms that the added canard variables do not make the problem intractable when the search is guided by uncertainty-aware surrogates.

4.2. Representative Pareto-optimal designs

Representative Pareto-optimal designs validated via the direct multidisciplinary model are listed in Table 4. From the results in Table 4, it can be seen that although the rear-mounted and three-surface configurations both have the potential to save mission fuel mass relative to the wing-mounted design, their implications and mechanisms are quite different.

Table 4. Representative Pareto-optimal designs following direct multidisciplinary validation.

Case	Cfg.	b_W (m)	AR_W	$X_{LE,W}$ (m)	b_H (m)	$X_{LE,H}$ (m)	b_C (m)	$X_{LE,C}$ (m)	Fuel (kg)	Empty Wt. (kg)	TOFL (m)	LFL (m)	Climb (min)	M_{cr}
A1	A	34.7	12.6	14.8	10.8	37.15	—	—	2645	14980	1318	1274	15.1	0.645
A2	A	35.2	13.1	15.2	10.9	37.15	—	—	2588	15120	1364	1296	15.4	0.652
B1	B	34.9	13.4	20.8	13.1	31.2	—	—	2472	15540	1378	1328	15.8	0.660
B2	B	35.3	13.7	21.4	13.7	31.6	—	—	2426	15770	1392	1344	15.6	0.666
C1	C	34.8	13.0	20.7	12.8	31.0	7.9	6.2	2388	15360	1336	1288	15.0	0.662
C2	C	35.1	13.2	21.1	13.0	31.3	8.3	6.8	2349	15470	1350	1292	14.8	0.667

The basic quantitative comparison of results can be expressed as

$$\Delta_r(q) = 100\frac{q_r - q_{A2}}{q_{A2}}, \tag{26}$$

in which the negative value means an improvement in fuel mass, empty weight, field lengths, and climb time, while a positive value means an improvement in cruise Mach number. As Eq. (26) implies, the difference between any Pareto design and its reference A2 counterpart can be converted into design consequence from Table 4. Specifically, the fuel mass saving of the rear-mounted B2 is 6.3%, at the cost of increasing empty weight by 4.3% and a slight increase in field length. On the other hand, the three-surface C2 saves 9.2% fuel mass and increases empty weight only 2.3%, reduces the take-off field length by approximately 1.0%, and improves climb time by 3.9%. Thus, in terms of design performance, the answer to the configuration problem is clearer in this case: the canard-equipped three-surface plane converts the aerodynamic benefit of rear-mounted engines to a better performance level.

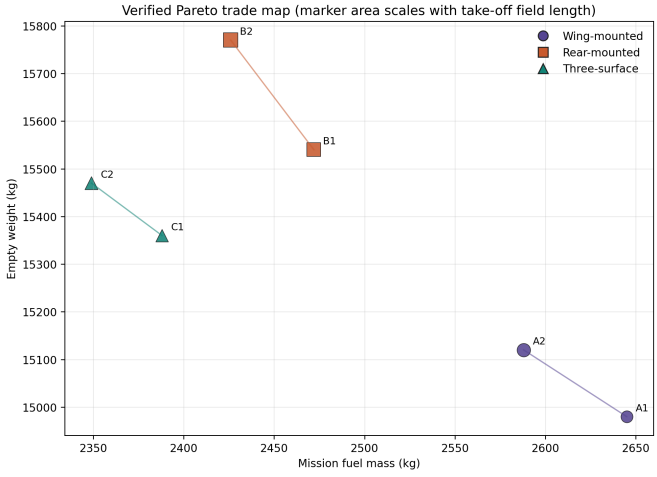

Figure 5. Verified Pareto trade map of representative designs. The updated colors separate the three architecture families, and marker area indicates take-off field length.

The relationship among the Pareto-optimal solutions is graphically depicted in Figure 5. In this diagram, the horizontal axis represents the mission fuel mass, and the vertical axis represents the empty weight; the area of each point is scaled by take-off field length. With respect to the reference, the two rear-mounted configurations move left to save fuel mass but upward to incur an increased empty weight. The three-surface configurations occupy the bottom left region relative to the rear-mounted two-surface points, which demonstrates the effect of using the canard in balancing the aircraft structure.

Representative optimized geometries are shown in Figure 6. The image demonstrates that the optimized solutions do not differ only in engine location; they also differ in wing placement, tail loading, and canard integration. The three-surface aircraft uses the canard as an active geometric contributor to longitudinal balance rather than as a decorative addition.

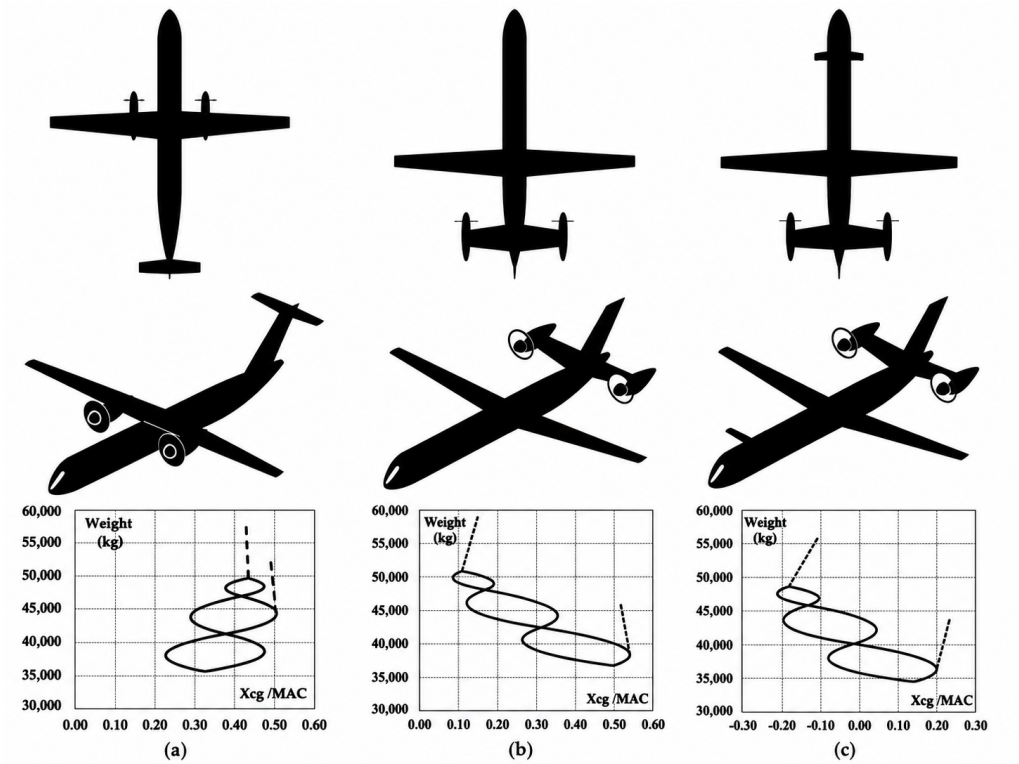

Figure 6. Representative optimized geometries associated with the three configuration families. The rendering is fully monochrome, preserving planform and perspective information through gray tone, contour emphasis, and geometry placement rather than colored airframe or propulsion details.

4.3. Interpretation of the trade-off

Wing-mounted configuration is still interesting due to its ability to produce bending relief through the location of engine. Thus, no penalty appears in terms of empty weight, as illustrated by the conventional configurations in Figure 5. Nevertheless, their high fuel mass reflects the need for higher installation drag to obtain familiar structures and less efficient cruise performance.

Rear propulsion demonstrates its aerodynamic advantage, confirming our expectations but also showing how its disadvantage works. Indeed, the elimination of nacelles from the wing yields a superior cruise drag polar and allows shifting the set of verified optimal solutions towards lower fuel mass. At the same time, the requirement to generate thrust by moving the mass further aft causes an increased load on the horizontal stabilizer and aft fuselage. Thus, rear propulsion produces a more fuel-efficient design at the expense of increased difficulty of optimization in terms of structural and field performance characteristics.

Three-lifting-surface configuration turns out to be the best compromise solution among all three verified families. As shown in Table 4, the optimum three-surface case is charac-

terized by the minimum fuel mass together with the best climbing time and reasonable field lengths. This happens not only because the canard produces lift, but because the new location of the moment center $X_{LE,C}$ makes the front lifting surface capable of providing the necessary moment without destabilizing longitudinal stability and producing bad aerodynamic interference.

The following operational score is suggested to evaluate the best representative design from each family:

$$P_{rj} = \begin{cases} 50 + 50\dfrac{q_j^{\max} - q_{rj}}{q_j^{\max} - q_j^{\min}}, & \text{for lower-is-better responses,} \\ 50 + 50\dfrac{q_{rj} - q_j^{\min}}{q_j^{\max} - q_j^{\min}}, & \text{for higher-is-better responses.} \end{cases} \tag{27}$$

Eq. (27) transforms the verified values to the range of 50–100 points for the purpose of comparison. No information about multi-criteria nature of the problem should be lost during this transformation: a certain configuration may be preferable in one response and poor in another.

Figure 7 shows the operational balance profile calculated according to Eq. (27). Conventional configuration is the most effective in terms of empty weight, the rear propulsion case is characterized by its capability to provide a higher cruise speed, and three surfaces win in terms of fuel mass, take-off field length, landing field length, and climbing time. Clearly, the choice of configuration is determined by design priorities; however, it should be mentioned that configuration C gives the highest operational balance in this case.

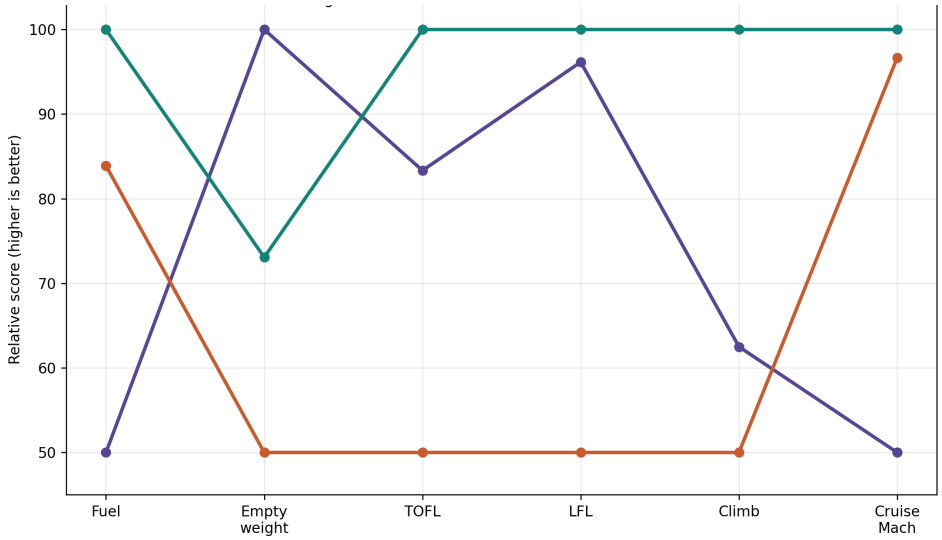

Figure 7. Operational-balance profile calculated based on representative optima. The higher value means higher relative performance after normalization of fuel mass, empty weight, field lengths, climbing time, and cruise speed.

4.4. Sensitivity analysis

The sensitivity analysis for a model following the Sobol method was conducted with the verified surrogates. Total influence of the variable x_i on the response Y is defined as

$$S_{T_i} = 1 - \frac{\mathrm{Var}_{\mathbf{x}_{\sim i}}[\mathbb{E}_{x_i}(Y \mid \mathbf{x}_{\sim i})]}{\mathrm{Var}(Y)}, \tag{28}$$

where $\mathbf{x}_{\sim i}$ refers to all the variables apart from x_i. One advantage of the Eq. (28) is that it captures the contribution from direct effects as well as interaction effects. For the aircraft design problem at hand, this feature is necessary since there is interaction among the wing

longitudinal location, the center of gravity displacement, the gear ground clearance, the static margin, and the performance of take-off/landing fields.

Table 5. Dominant design variables contributing to the main objective function and constraints after sensitivity analysis.

Response	Primary influence	Secondary influence	Physical significance
Mission fuel mass	Wing aspect ratio	Wing span	Efficiency of cruise phase controlled by drag due to induced lift and effective wing load.
Empty weight	Horizontal-tail span	Wing span	Structural growth dominated by tail stiffening and lifting surface size.
Take-off field length	Wing span	Wing longitudinal position	Low-speed lift and ground clearance determine runway requirement.
Static margin	Wing longitudinal position	Canard longitudinal position	Stability controlled by aerodynamic center and center of gravity distance.
Fuel capacity margin	Wing span	Wing aspect ratio	Volume and chord length distribution determine usable fuel capacity.
Landing-gear clearance margin	Wing longitudinal position	Tail position	Geometric relation determines the ground clearance for landing gear.

From the Table 5, it is found that despite the engine relocation to the aft position and the addition of a canard, the wing remains the dominant structure. It is because the wing span, its aspect ratio, and its longitudinal position affect all the major performance indicators, including efficiency, volume of fuel, and balance point. In addition, the horizontal tail becomes dominant for empty weight since the tail structure must cope with the aerodynamic trimming and aft positioning penalty.

Figure 8 visualizes the information in the table as the map of response-variable couplings. The implication of the diagram is that even though the canard longitudinal location is not the primary design variable for any response, it is the dominant secondary variable for static margin. Therefore, the canard design shall be considered as a variable of trim and stability rather than lifting area.

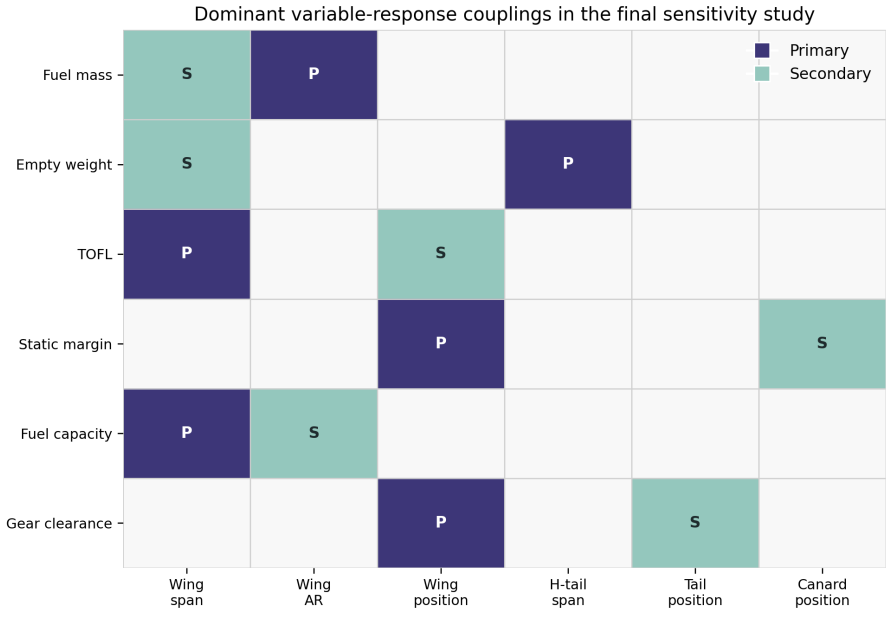

Figure 8. Dominant variable-response couplings obtained from the sensitivity analysis. "P" stands for the primary design driver, while "S" stands for the secondary driver for each response.

4.5. Significance of the approach from the methodological perspective

The introduction of surrogates completely shifts the character of the design exploration process. In exhaustive enumeration, all designs need to be considered on equal footing when they have no clear evidence that they are infeasible right after the first discipline analysis step. Our approach uses information obtained from infeasible samples, thus directing further analyses toward promising combinations located near the feasible Pareto bound-

ary. This explains the usefulness of our procedure for three-surface configurations, where the large design space would contain mostly infeasible wing-canard-tail combinations otherwise.

The verified solutions demonstrate the need for direct analysis of designs. Gaussian process models give sufficiently reliable predictions to facilitate the search. However, crucial aircraft-level conclusions should be reached using direct analysis because of possible dramatic changes in stability margin, gear clearance, and field length when approaching the boundary.

5. Conclusions

It was hypothesized that surrogate-assisted multi-objective optimization can find believable configuration advantages for advanced regional turboprop aircraft under the enforcement of aerodynamic, structural, stability, field performance, fuel capacity, and operating cost constraints. The hypothesis is confirmed. As a result, the number of direct multidisciplinary evaluations decreased by 72.8% for the wing-mounted variant, 93.6% for the rear-mounted variant, and 98.5% for the canard-equipped aircraft with three lifting surfaces. Simultaneously, the final validation errors were kept below 4.2% for the responses considered. Thus, the optimization approach is indeed not only faster than exhaustive configuration exploration, but also accurate enough for early stage analysis purposes.

Firstly, regarding rear-mounted propulsion, the verified results prove that relocation of the engines away from the wing decreases mission fuel mass by approximately 6.3% for the representative rear-mounted optimum B2 compared to the representative design A2. It is due to cleaner wing aerodynamics and lower installation drag. At the same time, the design is heavier by about 4.3% and shows worse indicators of the field lengths. Therefore, rear-mounted propulsion is advantageous only in cases where efficiency gain is significant enough to cover extra weight of the empennage and aft fuselage.

Secondly, the canard-equipped three-lifting-surface aircraft is proven to provide the best answer to the configuration question. The verified C2 design decreases the mission fuel mass by around 9.2% compared to A2. At the same time, empty weight grows by only about 2.3%, take-off and landing field lengths improve slightly, and climb time is reduced by 3.9%. It occurs since canard provides for redistribution of longitudinal lift force and reduces the trim burden provided that its span and longitudinal position lie within the stability corridor.

As it was explained before, the results are obtained due to sensitivity analysis which showed the physical reasons for the obtained outcomes. Specifically, the wing span, aspect ratio, and position influence on fuel behavior, empty weight is mostly controlled by horizontal tail span, and field performance is controlled mainly by static margin and wheel clearance. Therefore, canard position is the most important variable for the performance improvement because it contributes mostly to static margin.

For the given mission statement and constraints, the three lifting surfaces with rear propulsion configuration is the optimal solution of all three architecture family groups. For simplicity, the wing mounted configuration aircraft is the most straightforward, while the rear mounted two surface aircraft is the solution that offers clear reduction in fuel burn; however, the canard configuration aircraft is the one which shows the best balance of fuel, performance, climbing and cruise behavior. Further research should incorporate aeroelastic modeling, acoustic and vibration limitations, effects from propeller slip stream, and hybrid electric propulsion system integration.

Nomenclature

AR	aspect ratio
b	span
$\bar{c}$	mean aerodynamic chord
DOC^*	direct operating cost proxy
EI	expected improvement

HV	hypervolume
M_{cr}	cruise Mach number
MDA	multidisciplinary analysis
MDO	multidisciplinary design optimization
NSGA-II	Non-dominated Sorting Genetic Algorithm II
S_L	landing field length
S_{TO}	take-off field length
SM	static stability margin
W_{empty}	empty weight
X_{CG}	center-of-gravity longitudinal position
X_{LE}	leading-edge longitudinal position
X_{LG}	landing-gear longitudinal position

References

[1] Raymer, D. P. (2012). *Aircraft Design: A Conceptual Approach* (5th ed.). American Institute of Aeronautics and Astronautics.

[2] Torenbeek, E. (2013). *Advanced Aircraft Design: Conceptual Design, Analysis and Optimization of Subsonic Civil Airplanes*. John Wiley & Sons.

[3] Nicolai, L. M., & Carichner, G. E. (2010). *Fundamentals of Aircraft and Airship Design, Volume I: Aircraft Design*. American Institute of Aeronautics and Astronautics.

[4] Nicolosi, F., Corcione, S., Trifari, V., Cusati, V., Ruocco, M., & Della Vecchia, P. (2018). Performance evaluation and DOC estimation of an innovative turboprop configuration. In 2018 Aviation Technology, Integration, and Operations Conference (p. 3662).

[5] Nicolosi, F., Corcione, S., Della Vecchia, P., Trifari, V., & Ruocco, M. (2018, September). Aerodynamic design and analysis of an innovative regional turboprop configuration. In Proceedings of the 31st ICAS Conference (International Council of the Aeronautical Sciences), Belo Horizonte, Brazil (pp. 9-14).

[6] Nicolosi, F., Corcione, S., Trifari, V., & De Marco, A. (2021). Design and optimization of a large turboprop aircraft. Aerospace, 8(5), 132.

[7] Cusati, V., Corcione, S., Ciliberti, D., & Nicolosi, F. (2022). Design evolution and wind tunnel tests of a three-lifting surface regional transport aircraft. Aerospace, 9(3), 133.

[8] Corcione, S., Bonavolontà, G., De Marco, A., & Nicolosi, F. (2023). Downwash modelling for three-lifting-surface aircraft configuration design. Chinese Journal of Aeronautics, 36(6), 161-173.

[9] Roskam, J. (1985). *Airplane Design*. Roskam Aviation and Engineering Corporation.

[10] Gudmundsson, S. (2014). *General Aviation Aircraft Design: Applied Methods and Procedures*. Butterworth-Heinemann.

[11] Anderson, J. D. (2017). *Fundamentals of Aerodynamics* (6th ed.). McGraw-Hill Education.

[12] Martins, J. R., & Lambe, A. B. (2013). Multidisciplinary design optimization: a survey of architectures. AIAA journal, 51(9), 2049-2075.

[13] Simpson, T. W., Poplinski, J. D., Koch, P. N., & Allen, J. K. (2001). Metamodels for computer-based engineering design: survey and recommendations. Engineering with computers, 17(2), 129-150.

[14] Queipo, N. V., Haftka, R. T., Shyy, W., Goel, T., Vaidyanathan, R., & Tucker, P. K. (2005). Surrogate-based analysis and optimization. Progress in aerospace sciences, 41(1), 1-28.

[15] Forrester, A., Sobester, A., & Keane, A. (2008). Engineering design via surrogate modelling: a practical guide. John Wiley & Sons.

[16] Sóbester, A., Forrester, A. I., Toal, D. J., Tresidder, E., & Tucker, S. (2014). Engineering design applications of surrogate-assisted optimization techniques. Optimization and Engineering, 15(1), 243-265.

[17] Rasmussen, C. E., & Williams, C. (2006). Gaussian processes for machine learning the mit press. Cambridge, MA, 32, 68.

[18] Deb, K., Pratap, A., Agarwal, S., & Meyarivan, T. A. M. T. (2002). A fast and elitist multiobjective genetic algorithm: NSGA-II. IEEE transactions on evolutionary computation, 6(2), 182-197.

[19] Jones, D. R., Schonlau, M., & Welch, W. J. (1998). Efficient global optimization of expensive black-box functions. Journal of Global optimization, 13(4), 455-492.